# Measurements of OH, $H_2SO_4$, and MSA during TOPSE

R.L. Mauldin III[1], C.A. Cantrell[1], M.A. Zondlo[1], E. Kosciuch[1], B.A. Ridley[1], R. Weber[2], and F.E. Eisele[1,2]

1. Atmospheric Chemistry Division, National Center for Atmospheric Research, 1850 Table Mesa, Boulder, CO 80305
2. School of Earth and Atmospheric Sciences, Georgia Institute of Technology, 221 Bobby Dodd Pkwy, Atlanta, GA 30332

## Abstract

Data from OH, $H_2SO_4$, and MSA measurements performed during TOPSE are presented. Model simulations of OH results showed a tendency of the model to overestimate OH concentrations by a factor of two at the lower latitudes (<57° N) of the study, which moved toward agreement at the higher latitudes. Measurements of $H_2SO_4$ showed the highest concentrations at the lowest altitudes (<2000 m) and the lowest latitudes of the study. Larger $H_2SO_4$ concentrations observed at higher latitudes were accompanied at times by particle nucleation as indicated by the presence of UCN (ultra-fine condensation nuclei) with diameters of 3-4 nm. Concentrations of MSA were generally low with typical values of $<2x10^5$ molecule $cm^{-3}$. High concentrations were found in layers and were accompanied by other compounds such as $NO_x$ and $NO_y$ indicating MSA may also have an industrial source. Interferences from both cabin air leakage into the sample flow, and contamination of NO from a $HO_2/HO_2+RO_2$ instrument that shared a nitrogen line were detected after the study resulting in a limited OH data set.

## 1. Introduction

The hydroxyl radical is the primary oxidant in the lower atmosphere, responsible for controlling the buildup of numerous compounds of both anthropogenic and biogenic origins. In the lower troposphere, OH is formed primarily from the photolysis of ozone via the reaction sequence:

$$O_3 + h\nu\ (<330\ nm) \rightarrow O(^1D) + O_2(^1\Delta_g) \qquad (j(O(^1D))$$

$$\text{(R1)} \qquad O(^1D) + H_2O \rightarrow 2OH$$

thus, the [OH] depends directly upon the [$O_3$], actinic flux (number of photons), and the [$H_2O$].

The higher latitudes of the northern hemisphere present a unique environment for the study of the hydroxyl radical. The "springtime bloom" of ozone at these latitudes reported by *Penkett et al*. [1993] and investigated by the Tropospheric Ozone Production about the Spring Equinox, TOPSE, study [*Atlas et al.*, this issue] would be expected to produce enhanced levels of OH, thereby increasing the oxidizing capacity of this region. Alternatively, regions of anonymously low ozone concentrations [*Barrie and Platt*, 1997; *Hopper et al*., 1998] would be expected to have smaller oxidizing capacity due to low OH concentrations. Recently during the Investigation of Sulfur Chemistry in the Antarctic Troposphere (ISCAT) study, enhanced OH concentrations have been reported at the South Pole [*Mauldin et al*., 2001]. This enhancement in OH is attributed to unexpectedly high levels of NO, which originates through photochemistry in the snow pack [*Davis et al*., 2001]. High levels of $NO_x$ have been reported in the northern latitudes as well [*Honrath et al*., 1999, 2000a,b; *Jones et al*., 2000; *Ridley et al*., 2000] and were found to originate from the sunlit snow surface.

The main sulfur sources in the arctic are either volcanic or anthropogenic in origin. Sulfur is released into the lower troposphere mainly in the form of sulfur dioxide, $SO_2$ [*Barrie et al.*, 1989]. The $SO_2$ is then converted into sulfuric acid, $H_2SO_4$, in a multi-step process initiated by reaction with OH. Sulfuric acid is a key compound in the processes of particle nucleation and particle growth. It is also known that $H_2SO_4$ and particulate sulfate are the major constituents of arctic haze [*Jaeschke et al*., 1999]. Methane sulfonic acid, MSA, is thought to be produced mainly by the oxidation of dimethylsulfide, DMS. Which is emitted primarily by the oceans.

In this work we present measurements of OH, $H_2SO_4$, and MSA performed during the TOPSE study. OH results will be compared to steady state model simulations. Sulfuric acid measurements will be discussed in terms of latitudinal distributions and particle nucleation. MSA results are discussed in terms of possible sources in a region where natural DMS production should be low.

**2. Experimental Technique**

The selected ion chemical ionization mass spectrometry technique used for the measurement of OH, $H_2SO_4$, and MSA during TOPSE has been described elsewhere [*Eisele and Tanner*, 1991, 1993; *Tanner et al.*, 1997; *Mauldin et al.*, 1998, 1999a, 2001], and the reader is directed to those works for details. The instrument that was used to perform these measurements is a 4-channel mass spectrometer previously used in the NASA/GTE PEM-Tropics B campaign [*Mauldin et al.*, 2001] with a few modifications. The instrument measured OH, $H_2SO_4$ and MSA with the first (and most sensitive) mass spectrometer channel in both PEM-Tropics B and on TOPSE. The second channel,

previously used to measure dimethylsulfoxide, DMSO, in PEM-Tropics B, was replaced with a new inlet and ion source intended to measure $HNO_3$. The main change of relevance was the first-time use of the third mass spectrometer channel to measure $HO_2$ and $RO_2$ [*Cantrell et al.* this issue]. This channel has its own inlet, ion source, reaction region, mass spectrometer, and ion detector. The only real link between this channel and the OH channel was a common vacuum system (housing, pumps, etc.), a shared data collection system, and a shared nitrogen cylinder. These shared components significantly reduced the instrument's space and weight requirements compared to 3 or 4 separate mass spectrometer systems. Unfortunately, two unexpected problems arose with this new instrument, the first involving an interference between the OH and $HO_2$ channels and a second involving a leak in the OH calibration shutter mechanism.

Despite considerable effort to prevent any type of interactions between ions, gases, pumping, or electrical components on individual channels, NO gas being used in the $HO_2$ and $RO_2$ measurement channel managed to get back upstream to a common nitrogen line that also fed the OH channel. This NO caused enhanced OH values by converting some ambient $HO_2$ into OH inside of the OH measurement channel. The problem was not clearly identified until the $5^{th}$ deployment, after which several sets of check valves were placed in the nitrogen lines to remove the possibility of NO back streaming into the main $N_2$ flow. This contamination resulted in the loss of nearly all data from the $5^{th}$ deployment. Prior to the $5^{th}$ deployment regulator pressures for the NO source gas were typically lower so that the ability of NO to enter the main $N_2$ flow and be transported into the OH channel was far less and not detectable in the calibrations. Ambient calibrations provide a means of detecting the introduction of relatively large

amounts of NO, but since the OH calibration source only produces OH and $HO_2$ in a ratio of 1:1 instead of in the ambient ratio of 1:10 to 1:100, small NO interferences are difficult to discern. To summarize, most of the data from deployment 5 has been removed except for a short time after the problem was found and NO was turned off. Data after deployment 5 and below 3000 meters should be correct (see below). We have no direct evidence that data before deployment 5 is tainted and we think that most of it is good, but we cannot rule out the possibility of NO interferences, particularly in the first 1 or 2 deployments where many measured OH values were very high, and many $HO_2/RO_2$ parameters were being adjusted.

A second leak problem also occurred involving a leak of cabin air through a slit in the side of the OH inlet that was not discovered until after the end of the mission. The leak occurred through a mechanical element that opened a shutter, which controlled a beam of 184.9 nm UV light used to generate OH from ambient $H_2O$ during calibration periods (see Figure 1). While OH was generated across the width on the 5 cm diameter inner inlet, OH was only sampled from the very central portion of the inlet flow. Thus, while cabin air could reach the 5 cm diameter inlet whenever the cabin pressure was above the inlet's ram air pressure, it could only reach the central sampled portion of the inlet flow at relatively high altitudes and high leak rates. Fairly direct evidence of this leak can be seen in flight 20, when the cabin pressure was abruptly reduced in the middle of a level high altitude flight leg and OH went from near zero to a measurable concentration. The innermost OH sampling inlet is centered in the 5 cm diameter inlet and is only about 4 cm behind the slit where cabin air could enter the inlet. Air flow in the inlet without a leak has previously been well characterized [*Eisele et al.,* 1997] and is

believed to be quite laminar with no boundary layer air from the walls mixing into the central region of the 5 cm inlet. With the leak, TOPSE OH data obtained just prior to a calibration measurement, provides a means of assessing when air leaking through the calibration lamp slit could reach the measurement region of the inlet. During this period the calibration lamp is on but the shutter closed. Leaked cabin air is exposed to the UV radiation as it passes between the mercury lamp source and the closed shutter, generating OH, which is then transported into the 5 cm inlet. Thus an increase in OH is observed after the mercury lamp is turned on with the shutter closed when the leak rate was sufficient to transport cabin air to the central sampled region of the 5 cm inlet. Figure 2 is a plot of the observed increase in OH with the mercury lamp turned on and the shutter closed divided by the expected amount of OH to be formed versus altitude. The altitude variation suggests the interference from this leak goes to zero at about 3000 meters. In Figure 2, the OH values are divided by water concentrations because the OH formed by the Hg lamp should scale with $H_2O$. The 6 zero values between 3000 and 4000 m correspond to no measurable increase in OH being observed with the lamp on and shutter closed, despite relatively high $H_2O$ concentrations that produce much larger signals. The actual percentage of cabin air reaching the measurement region is difficult to determine, but measurements of the gas flow through the leak as a function of pressure combined with assuming a worst case mixing geometry suggests a maximum of about 30% of the sample air at maximum altitude could be cabin air (probably the actual mixing ratio is less than 20%). From the previous extrapolation, this would be expected to drop to just a few percent at 4000-4500 meter altitude. Thus, compounds not expected to react differently with cabin air than in ambient air, such as $H_2SO_4$ and MSA, are expected to be

reduced just by a small dilution factor at low altitudes. At the highest altitudes, enhanced loss due to increased turbulence could further reduce the measured values of these two compounds, but it is difficult to see that the losses would reach a factor of 2. Therefore, the positive error bars on $H_2SO_4$ and MSA have been increased to + 100% at high altitudes.

Since OH can react very differently with cabin air compared to ambient air in the 0.04 seconds or so before its measurement, the latter argument cannot be directly applied to its measurement. Only a small amount of cabin air containing, for example, a relatively high concentration of organics or NO could have an exaggerated effect. Figure 2, however, suggests not just that the leak interference should be low at 4000 meters, but that it is at or below zero by 3000 meters. This is exactly the type of behavior one would expect of such a leak. By 3000 meters, the leak flow is only about 3 to 4% of the total 5 cm diameter inlet flow. The leak should also enter the inlet with a much lower flow velocity than the inlet flow, having lost both flow speed and total mass flow relative to the inlet flow due to the decrease in the difference between the ambient and cabin pressures. Thus, a fairly rapid transition is expected from significant mixing to no mixing in the central portion of the flow from which OH is sampled, as the air from the leak is pushed along the inlet tube wall by the much larger and faster ambient inlet flow.

While these arguments provide a strong indication that the OH data below about 3000 meters should be unaffected by the leak, an independent and more direct indication can be seen by comparing the calibrations obtained from different field studies. The calibration factor for the OH measurement depends on: the reaction rate of $NO_3^-$ with $H_2SO_4$, an imprecisely known but presumably a fixed natural constant (these ion

reactions have a very small temperature dependence); the reaction time, which is controlled by well monitored flows and electric fields; the difference in detection efficiency for 2 fairly similar ions (quite constant); and sampling losses, which appear to be only pressure dependent. Since there are essentially no variables that will change the calibration constant which are not controlled and held constant other than ambient pressure, the calibration constant is quite consistent for a given pressure altitude, both between successive flights and even between missions that are years apart. Essentially the identical instrument and calibration technique were used on TOPSE as were used during the NASA/GTE TRACE-P study (except that the leak was finally found and stopped during the very early part of TRACE-P), thus the calibrations should be the same. Figure 3 is a semi-log plot of individual calibration constant measurements from both TOPSE and TRACE-P as a function of ambient pressure plotted along with a line for the average and 2 lines that define one half and 2 times the average calibration constant determined for TRACE-P. It can be seen that the calibrations are consistent with the maximum difference between calibration constants at well under 10% below 3000 m. While the average calibrations are very similar, the scatter in the calibrations is quite different above 3000 meter (680 mb). Most of the TRACE-P calibrations are within a factor of 1.5 of the mean value with nearly all values within a factor of ± 2. Much of this scatter is due to changing water concentrations during the calibration, and in some cases probably due to shutter slit width setting errors that could not be verified and were thus left in the data set. In general, the scatter in the measured OH concentration is smaller than the scatter in the calibration if OH is well above the detection limit. The increase in scatter is due to the strong dependence of the calibration upon airspeed, turbulence, and knowledge

of $H_2O$ concentrations. The TOPSE calibrations are expected to have a similar scatter. At pressures above 680 mb nearly all of the TOPSE points fall between the lines as expected, but below 680 mb most of the points are outside of the lines and often a factor of 10 or more above or below the expected value. The calibration points below the lines are believed to be due to small amounts of NO leaked from the nearby $HO_2$ measurement getting into the inlet via the cabin air leak. In fact, all of the calibrations done when $HO_2$ was being measured (which used flows of pure NO, and $SO_2$) were within or below the two lines. Calibration factors above the two lines are thought to result from the destruction of OH by some reactive compound in the cabin air which probably varies with cabin heating, cabin air residence time and other factors which can not be replicated. Calibration done when $HO_2 + RO_2$ was being measured (which used diluted flows of NO and $SO_2$) appear to be distributed randomly throughout the data, showing no particular influence. Below 3000 meters (>680 mb), $HO_2$ measurements appeared to have no effect on the OH calibration, with a possible hint of a shift in calibration right at 680 mb. Calibrations near 800 mb are actually slightly higher than expected despite the fact that several of these were measured while $HO_2$ was being measured. These add some additional support to the sharp cutoff of any leak interferences at about 680 mb.

These results suggest that all OH data at pressures below 680 mb (above 3000 meters) are highly questionable and have thus been discarded. At pressures near 680 mb, data was only removed when $HO_2$ was being measured, but of course some additional caution should be exercised when using data near this transition point, although the remaining 680 mb data are believed to be good. At pressures above 680 mb, the OH data are not expected to be affected by this inlet leak. The calibration used from 680 mb to

1000 mb was that obtained from calibrations during TOPSE, which are very close to TRACE-P values. Calibrations used to calculate $H_2SO_4$ and MSA measured at pressures below 680 mb (altitudes >3000 m) are those measured on TRACE-P. Calibrations from the previous PEM-Tropics B were not used because the electric fields used to guide and collect ions were changed.

Another issue that should be briefly addressed at this point is the potential influence of this leak on previous missions. This calibration shutter design has been used previously only once before during PEM-Tropics B on the NASA P-3b aircraft. The instrument configuration was quite similar on PEM-Tropics B, except that no $HO_2$ or $RO_2$ channel was installed, and [NO] within the aircraft was probably quite low. Also, for much of the mission, an O-ring was used in the calibration shutter, which might have sealed off the cabin air leak and diverted the flow away from the calibration light entrance slit, and thus the OH inlet. The O-ring which was only intended to keep a window from getting wet if the aircraft flew through wet clouds was removed later in PEM-Tropics B because of problems with the shutter sticking. The PEM-Tropics B calibrations, however, are more similar to TRACE-P rather than TOPSE. They are not highly scattered, but rather quite well behaved. At least during the end of PEM-Tropics B, some air should have been leaking out of the inlet, but it appears to have had little effect on the calibration nor, presumably, on the measurement. This observation is probably because little cabin air actually reached the central sampling area of the inlet, as was the case in TOPSE. If this air did not contain a highly reactive compound, then it should have had only a small effect on the OH measurement, reducing the measured OH slightly due to dilution. Fortunately, dilution should have had the same effect on both

calibration and measurement for a given altitude. Thus, since any leak effects were too small to be identified, and leak influences should already have been taken into account by their inclusion in the calibration, the existing PEM-Tropics B data remains our best estimate of OH, $H_2SO_4$ and MSA concentrations during that study.

The same data-taking scheme was used in this study as was used in PEM-Tropics B. OH, $H_2SO_4$, and MSA values are reported once every 30 s. Error limits of ±46.0% (2 sigma and correspond to the 95% confidence level) were calculated referring to the total systematic and random errors for a given measurement. The total reported errors are ± 46% for data obtained at pressures greater than 680 mb and a factor of ± 2 for $H_2SO_4$, and MSA data obtained at pressures less than 680 mb. The increase in uncertainty for $H_2SO_4$ and MSA at pressures below 680 mb (above 3000 m) reflects the use of the PEM-Tropics B calibration coefficients, and the uncertainty in dilution due to the cabin air leak.

## 3. Results

With the exception of the flights in deployment 5 discussed above, OH and $H_2SO_4$ values are reported for each flight. MSA was measured periodically in deployment 4, and continuously throughout deployments 6 and 7. $H_2SO_4$ and MSA values are given at all altitudes, while the OH has been limited to pressure altitudes greater than 680 mb (> 3000 m). Data may be downloaded from the data archive on the TOPSE web site, http://topse.acd.ucar.edu.

### 3.1 OH Measurements and Modeling

Photochemical box model simulations of the TOPSE OH data were performed using a model developed at NCAR. The model used for these simulations is described fully elsewhere [*Cantrell et al.*, this issue]; thus only relevant details will be discussed

here. The model inputs were one-minute averages of the species measured aboard the aircraft that affect radical concentrations ($O_3$, $j(O_3)$, NO, CO, $H_2O_2$, hydrocarbons, etc). Reaction rates were based on the 1997 NASA JPL [*DeMore et al*., 1997] and the 1997 J. Phys. Chem. Ref. Data [*Atkinson et al.*, 1997] recommendations. An initial comparison of OH measurements and model results for all flights during TOPSE can be seen in Figure 4a. Also shown is a 1:1 correlation line for reference. A linear fit to this data yields a slope of 0.41, indicating a tendency of the model to over-estimate OH concentrations.

It is worth noting that there is a cluster of data located near 0 on the x or modeled OH axis where the measured OH is quite higher. This cluster, when looked at more closely, is comprised mainly of data obtained during the first and part of the second deployment. A more sensitive analysis of the differences is to look at the ratio of measured to modeled values. Figure 4b is a plot of the ratio of measured to modeled OH concentrations shown in Figure 4a versus altitude. A ratio of one indicates perfect agreement. The high values of the first two deployments are more clearly seen. As was stated earlier anomalously high OH values were observed during deployment 5, and were found to result from NO back flowing into the $N_2$ supply line for the OH instrument. Check valves were installed after deployment 5 to prevent this back streaming. There is no direct evidence of this contamination in data prior to deployment 5, however caution must be exercised. Data from the first and part of the second deployments exhibit much larger OH concentrations than would be expected for a time of year when actinic flux is small. If the data from the first two deployments are eliminated from Figure 4a, the calculated slope increases to 0.50, still indicating a general tendency of the model to overestimate the [OH] by a factor of 2. From Figure 4b, it can be seen that there is a

slight trend of the model to underestimate OH concentrations at sea level, when compared to measurements, which then changes to an overestimation with increasing altitude. At ~3000 m, this overestimation has risen to approximately a factor of two. While there were many low level legs (< 500 m) flown throughout the mission, the majority of OH data were obtained at higher altitudes. It is the data obtained at these higher altitudes that are causing the slope of Figure 4a to go towards lower values, indicating an overall trend to over estimate OH. One explanation for the higher model values is the presence of biogenic compounds that act as sinks for OH, particularly at lower latitudes, but are not measured and thus, not included in the model.

The latitudinal dependence of the agreement of measurements with model simulations was also examined. Figure 5 is a plot of the ratio of measured to modeled OH concentrations versus latitude for all TOPSE deployments. Again the high values of the first two deployments are obvious. Also apparent is a trend of the model to overestimate OH concentrations at lower latitudes, which moves towards agreement or a slight underestimation at higher latitudes. It is important to note that this trend is present in deployments 6 and 7 (after the check valves were installed) as well as deployments 3, 4, and 5 (before check valves were installed). Thus, there appears to be no seasonal dependence to this trend.

One of the several interesting observations made during the TOPSE mission, was the occurrence of ozone, $O_3$, depletion within the boundary layer. Figure 6 is a plot of measured OH and $O_3$ during a low ozone event. Altitude is plotted in the upper graph. As the plane descends into the boundary layer, the [$O_3$] dropped from ~75 to less than 1 ppbv. During this time, the OH fell from an average value of ~$4x10^5$ molecule $cm^{-3}$ to

~1x$10^5$ molecule $cm^{-3}$. This factor of four reduction in OH might seem small for such a large change (over a factor of 100) in ozone, a parameter that directly controls the OH production. Also shown in Figure 6 is the model simulated OH during this period. As can be seen the factor of 4 change in [OH] is also predicted by the model. In fact the overall agreement between measurement and model is quite good despite the fact this is a highly chemically perturbed environment.

### 3.2 $H_2SO_4$ Measurements

Sulfuric acid was measured throughout the entire TOPSE mission, with concentrations being reported at all altitudes. Typically concentrations were low with values ranging from 0.5 x $10^6$ to 1.5 x $10^6$ molecule $cm^{-3}$. Both seasonal and altitudinal dependences can be noted. Figure 7 is a plot of $H_2SO_4$ concentrations versus altitude for all deployments during TOPSE. The data have been separated into low (< 57 °N, Figure 7a) and high (>= 57 °N, Figure 7b) latitude values and averaged into 500 m segments. Due to instrument startup and shutdown considerations, no data was acquired for the lowest altitude bin at low latitudes. As can be seen, overall, higher $H_2SO_4$ values were observed in the lower latitude regions of the study. Typically also, the highest values are observed at the lowest altitudes. This observation is consistent with increased $SO_2$ ground sources at lower latitudes.

The seasonal dependence of the $H_2SO_4$ can also be seen in Figure 7. At high latitudes, the lowest concentrations are observed during the first two deployments. As the study continues, the observed concentrations generally increase up to deployment 6 where the largest concentrations were observed. On deployment 7 there was a dramatic decrease in [$H_2SO_4$] observed at all altitudes. This decrease was seen at both high and

low latitudes. The large excursions observed at high latitudes and higher altitudes during deployments 3 and 6 appear indicative of some perturbation of either dynamics or an $H_2SO_4$ source such as $SO_2$.

A case for particle nucleation together with high $H_2SO_4$ concentrations is explored here based upon an event that occurred on flight 10 during deployment 2. Shown in Figure 8 is a plot of $H_2SO_4$ values together with ultra fine condensation nuclei, UCN, concentrations. As can be seen during the time period 2015 to ~2030, $H_2SO_4$ values dramatically increase rising from $<1 \times 10^6$ to $\sim 10 \times 10^6$ molecule $cm^{-3}$. During this time an increase in the total UCN concentration by over a factor of 10 is also observed, indicating the presence of older, more aged UCN. The correlation between $H_2SO_4$ and total UCN is readily apparent. It is during this time, that the concentrations of nanoparticles (particles with diameters < 8 nm) are seen to rise. The peaks of the UCN with diameters of 3-4 nm reveal the presence of very young, recently nucleated particles that have not had the time to grow or become incorporated into larger particles. After 2030, the $H_2SO_4$ falls back to levels of $<1 \times 10^6$ molecule $cm^{-3}$, and total UCN concentration drops by approximately a factor of 20. Nanoparticle concentrations fall to essentially zero.

### 3.3 Methane Sulfonic Acid Measurements

MSA was not measured until deployment 4 of the mission and then only periodically for that deployment. Concentrations are reported for all flights and at all altitudes for deployments 6 and 7. Typically concentrations were quite low with values near $1\text{-}2 \times 10^5$ molecule $cm^{-3}$. When larger concentrations were observed, they tended to be in layers. The data shown in Figure 9, exemplifies a typical MSA event. Figure 9a

shows measured MSA concentrations versus time for a flight from Winnipeg, Manitoba to Churchill, Manitoba. At ~2252 UTC (~59 °N), as the aircraft was descending, the [MSA] abruptly spiked over a factor of 300 from $<2 \times 10^5$ to $6 \times 10^7$ molecule $cm^{-3}$. A similar, but larger scale event is observed at ~2330 as the aircraft ascends from the low level leg, with the [MSA] changing by almost a factor of 1000. Figure 9b is a plot of altitude versus the same MSA data shown in 10a. The layering of the large concentrations of MSA is quite apparent.

**4. Conclusions**

TOPSE was the first use of the four channel mass spectrometer system with the $HO_2/RO_2$ instrument installed. Although considerable effort to prevent interferences between the three instruments installed on the mass spectrometer system, contamination of the OH instrument from the $HO_2/RO_2$ instrument still occurred. This interference was noted on deployment 5 and measures were taken to eliminate it on deployments 6 and 7. There is no direct evidence of this contamination prior to deployment 5, however care must be taken in the use of these values. Data obtained during the first two deployments show elevated values of OH when the low actinic flux at that time of year is considered.

Additionally, a problem with a leak of cabin air into the sample flow, through a tube used to control the shutter on the calibration assembly, was discovered. Due to the extreme reactivity of the OH radical, even small amounts of cabin air being introduced into the sample flow can cause large interferences in OH measurements. This interference led to the OH data obtained at altitudes with pressures below 680 mb (> ~3000 m) being removed from the data set. As $H_2SO_4$ and MSA are far less chemically reactive, the cabin air leak into the sample flow will only result in dilution of these species during their

measurement. The worst case mixing scenario (maximum altitude or maximum pressure differential between cabin and ambient) suggests a 30% contribution of cabin air. This contribution is expected fall to a few percent at the 4000-4500 m altitude range. Thus, $H_2SO_4$ and MSA are reported at all altitudes with an increased uncertainty at pressures below 680 mb.

Despite the above problems, interesting OH results were obtained at lower altitudes. The other parameters measured during TOPSE provide an extensive data set for comparison with OH measurements. As shown in Figure 4, comparison with an NCAR steady state photochemical model reveals that the model tends to overestimate the [OH] when compared to measurements. This trend while not as large as seen in the present study has been observed before [*Mckeen et al.*, 1997; *Mauldin et al*., 1998, 1999a, 2001]. With the exception of the work by *Mauldin et al*. [2001], the discrepancies between measurements and model were explained by incomplete measurements of actinic flux or OH sinks. In the work of *Mauldin et al*. [2001], complete j-value measurements were included in the model, however the same overestimation trend was still observed. The authors of that work pointed out a need for more complete or better measurements of species that control OH production. The argument for measurements of additional OH sinks (other than those made during the study) can be made from the data shown in Figure 5. From this plot it can be seen that the model experiences the largest overestimation of OH at the most southern latitudes of the study. At the northern most latitudes, the model generally agrees with measurements. It is in the southern latitudes where anthropogenic and biogenic emissions are the greatest. It is also this region where one would expect to find compounds such as partially reacted hydrocarbons, oxygenated

hydrocarbons, etc; which were not measured and which would act as OH sinks. Without the incorporation of these additional sinks for OH, the model will continue to overestimate OH concentrations in these regions. In northern regions where these sinks are not as prevalent, the model generally does well. This fact is evidenced by the data shown in Figure 6. These low ozone events occurred at ~82 °N, a latitude where anthropogenic and biogenic influences should be at a minimum. Even under highly perturbed conditions for OH production, the model shows quite reasonable agreement with measurements.

Increased emissions at lower latitudes are also evident in the $H_2SO_4$ data. The largest $H_2SO_4$ concentrations were found at the lowest altitudes at the lower latitudes. The decrease in $H_2SO_4$ concentrations with increasing altitude seen in Figure 7a is consistent with a $H_2SO_4$ source being emitted at the surface and mixing upwards. Sulfuric acid has a much shorter lifetime than its source compounds, being readily scavenged onto particles. Thus, the [$H_2SO_4$] would be expected to decrease as its source from the surface is diluted as it is mixed upward. It should be pointed out that there was little direct correlation with $SO_2$ concentration found. This observation is not unexpected as the concentration of gas phase $H_2SO_4$ is dependent upon production and loss. Production includes both [$SO_2$] and [OH]. Long term exposure of $SO_2$ to OH is a major sink, thus OH and $SO_2$ should be anti-correlated. Loss terms include scavenging by particles, rainout, and surface deposition. As the study moved from early February to May, the [OH] increased as sun angle increased. It is this increase that is presumably the cause for the increasing amounts of $H_2SO_4$ observed during deployments 1-6. The cause of the sudden drop in $H_2SO_4$ observed in deployment 7 is unknown. One could speculate that

the use of fuels that produce $SO_2$ drops about this time of year in the northern hemisphere. Measurements of particle sulfate show the same trend, increasing until deployment 5 or 6 and then decreasing. The large excursions seen at higher altitudes in the high latitude plot for deployments 3 and 6 may be due to volcanic activity. These excursions are accompanied by large particle concentrations [*Wang et al*., this issue] consisting of mostly aged UCN. However there were occurrences of new particle nucleation. The data shown from flight 10 shown in Figure 8 demonstrates one of these occurrences. While the bulk of the particle distribution lies with the larger UCN, there are two instances during the high $H_2SO_4$ event where the 3-4 nm UCN reached concentrations of 200-300 $cm^{-3}$, indicating the presence of very recently formed particles. It is interesting to note that the $H_2SO_4$ concentrations during which this nucleation event occurred were not that large. As pointed out by *Wang et al.* [this issue] the mechanism for new particle formation likely involves $H_2SO_4$, however the concentrations are not sufficient for the formation to be explained by bi-molecular $H_2SO_4/H_2O$ theory.

MSA was measured periodically through the middle of the study, and on every flight of deployments 6 and 7. Typical concentrations were essentially zero with the exception of plumes where the concentrations would rise into the high $10^7$, low $10^8$ molecule $cm^{-3}$ range. These plumes were encountered as layers for the most part as shown in Figure 9. These layers were almost always accompanied by $NO_x$, $NO_y$ compounds indicating that these were probably pollution events. MSA is typically thought to have marine origins being produced via the oxidation of dimethyl sulfide, DMS, by OH [*Berresheim et al.*, 1995]. Additionally, appreciable gas phase concentrations are usually accompanied by lower (<20%) relative humidities [*Mauldin et*

*al.*, 1999b] and are interpreted as arising from particle evaporation of MSA. The large values reported here were seen under much higher (>50%) relative humidities. The fact that larger concentrations were accompanied by $NO_x$, $NO_y$ compounds would indicate that the MSA might have an industrial source. Whether MSA is produced directly or from further oxidation of a combustion byproduct cannot be discerned. While it is not too far of an extrapolation to see that MSA could be formed in industrial processes (sulfur compounds, hydrocarbons, and combustion), these are the first measurements of gas phase MSA in pollution plumes made in the free troposphere that these authors know of. The fact that the large MSA concentrations were observed under much high relative humidity conditions than previously reported, indicate that the vapor pressure of MSA above particles is highly dependent upon the particle composition, or there is a very high production rate in the plumes.

## 5. References


Atkinson, R., *et al.*, Evaluated kinetic and photochemical data for atmospheric chemistry: Supplement VI, IUPAC subcommittee on gas kinetics data evaluation for atmospheric chemistry, *J. Phys. Chem. Ref. Data*, *26*, 1329-1499, 1997.

Atlas et al. this issue

Barrie, L.A., G. den Hartog, J.W. Bottenheim, and S. Landsberger, Anthropogenic aerosols and gases in the lower troposphere at Alert Canada in 1986, *J. Atmos. Chem.*, *9*, 101-127, 1989.

Barrie, L.A., and U. Platt, Arctic tropospheric chemistry: an overview, *Tellus*, *49b*, 450-454, 1997.

Berresheim, H., P. Wine, and D. Davis, in H. Singh Ed., Sulfur in the Atmosphere, Van Nostrand Reihold, 251-307, 1995.

Davis, D., J.B. Nowak, G. Chen, M. Buhr, R. Arimoto, A. Hogan, F. Eisele, L. Mauldin, D. Tanner, R. Shetter, B. Lefer, and P. McMurry, Unexpected high levels of NO observed at the South Pole, *Geophys. Res. Lett.*, *28*, 3625-3628, 2001.

DeMore, W.B., S.P. Sander, D.M. Golden, R.F. Hampson, M.J. Kurylo, C.J. Howard, A.R.Ravishankara, C.E. Kolb, and M.J. Molina, Chemical kinetics and photochemical data for use in stratospheric modeling, *in evaluation 12*, *JPL Publ. 97-4*, 266 pp., Jet Propul. Lab., Pasadena, Calif., 1997.

Cantrell, C. A., et al., Peroxy Radical Behavior during the Winter-to-Spring Seasonal Transition at Middle to High Latitudes during TOPSE, this issue

Eisele, F.L., and D.J. Tanner, Ion-assisted tropospheric OH measurements, *J. Geophys. Res.*, *96*, 9295-9308, 1991.

Eisele, F.L., and D.J. Tanner, Measurement of the gas phase concentration of $H_2SO_4$ and methane sulfonic acid and estimates of $H_2SO_4$ production and loss in the atmosphere, *J. Geophys. Res.*, *98*, 9001-9010, 1993.

Eisele, F.L., R.L. Mauldin III, D.J. Tanner, J. Fox, T. Mouch, and T. Scully, An inlet/sampling duct for airborne OH and sulfuric acid measurements, *J. Geophys. Res.*, *102*, 27993-28001, 1997.

Honrath, R.E., M.C. Peterson, S. Guo, J.E. Dibb, P.B. Shepson, and B. Campbell, Evidence of $NO_x$ production within or upon ice particles in the Greenland snow pack, *Geophys. Res. Lett.*, *26*, 695-698, 1999.

Honrath, R.E., M.C. Peterson, M.P. Dziobak, J.E. Dibb, M.A. Arsenault, and S.A. Green, Release of $NO_x$ from sunlight irradiated midlatitude snow, *Geophys. Res. Lett.*, *27*, 2237-2240, 2000a.

Honrath, R.E., S. Guo, M.C. Peterson, M.P. Dziobak, J.E. Dibb, and M.A. Arsenault, Photochemical production of gas phase $NO_x$ from ice crystal $NO_3^-$, *J. Geophys. Res., 105*, 24,183-24,190, 2000b.

Hopper, J.F., L.A. Barrie, A. Silis, W. Hart, A. Gallant, and H. Dryfhout, Ozone and meteorology during the 1994 Polar Sunrise Experiment, *J. Geophys. Res.*, *103*, 1481-1492, 1998.

Jaeschke, W., T. Salkowski, J.P. Dierssen, J.V. Trumbach, U. Krischke, and A. Gunther, Measurements of trace substances in the Arctic troposphere as potential precursors and constituents of Arctic haze, *J. Atmos. Chem.*, *34*, 291-319, 1999.

Jones, A.E., R. Weller, E.W. Wolff, and H.-W. Jacobi, Speciation and rate of photochemical NO and $NO_2$ production in Antarctic snow, *Geophys. Res. Lett.*, *27*,

345-348, 2000.

Mauldin, R.L. III, G.J. Frost, F.L. Eisele, S. Madronich, S.J. Flocke, and A.S.H. Prevot, New insights on OH: Measurements around and in clouds, *Geophys. Res. Lett.*, *24*, 3033-3036, 1997.

Mauldin, R.L. III, D.J. Tanner, G.J. Frost, G. Chen, A.S.H. Prevot, D.D. Davis, and F.L. Eisele, OH measurements during ACE-1: observations and model comparisons, *J. Geophys. Res.*, *103*, 16713-16729, 1998.

Mauldin, R.L. III, D.J. Tanner, G.J. Frost, G. Chen, A.S.H. Prevot, D.D. Davis, and F.L. Eisele, OH measurements during PEM-Tropics A, *J. Geophys. Res.*, *104*, 5817-5827, 1999a.

Mauldin, R.L.III, D.J. Tanner, J.A. Heath, B.J. Huebert, and F.L. Eisele, Observations of $H_2SO_4$ and MSA during PEM Tropics, *J. Geophys. Res.*, *104*, 5801-5815, 1999b.

Mauldin III, R.L., F.L. Eisele, D.J. Tanner, E. Kosciuch, R. Shetter, B. Lefer, S.R. Hall, J.B. Nowak, M. Buhr, G. Chen, P. Wang, and D. Davis, Measurements of OH, $H_2SO_4$, and MSA at the South Pole during ISCAT, *Geophys. Res. Lett.*, *28*, 3629-3632, 2001.

Mauldin, R.L. III, F.L. Eisele, D.J. Tanner, C.A. Cantrell, E. Kosciuch, J.B. Nowak, G. Chen, L. Wang, D. Davis, B.A. Ridley, and B. Lefer, Measurements of OH aboard the NASA P-3 during PEM-Tropics B, *J. Geophys. Res.*, in press 2001.

McKeen, S.A., *et al.*, Photochemical modeling of hydroxyl and its relationship to other species during the tropospheric OH photochemistry experiment, *J. Geophys. Res.*, *102*, 6467-6493, 1997.

Ridley, B.A., J. Walega, D. Montzka, F. Grahek, E. Atlas, F. Flocke, V. Stroud, J. Deary, A. Gallant, H. Boudries, J. Bottenheim, A. Anlauf, D. Worthy, A.L. Sumner, B.

Splawn, and P. Shepson, Is the Arctic surface layer a source and sink of $NO_x$ in winter/sring?, *J. Atmos. Chem.*, *36*, 1-22, 2000.

Tanner, D.J., A. Jefferson, and F.L. Eisele, Selected ion chemical ionization mass spectrometric measurement of OH, *J. Geophys. Res.*, *102*, 6415-6425, 1997.

**Figure Captions**

**Figure 1**. Schematic diagram of the inlet, ion reaction region, and calibration assembly. The detail of the calibration assembly shows the shutter control tube, which at times allowed cabin air to leak into the sample flow (see text).

**Figure 2**. Plot of the relative observed increase in OH during calibrations with the calibration shutter closed. These increases are the result of cabin air passing in front of the mercury lamp where it is photolyzed, blowing past the shutter and then entering the sample flow. The zero intercept suggests that this leakage should not affect data taken at pressures above 680 mb.

**Figure 3**. Plot of individual calibrations measured in the TOPSE mission together with those obtained from the NASA GTE TRACE-P study. The calibrations from TOPSE above 680 mb are for the most part within the error limits of those obtained during TRACE-P. The increased scatter at pressures below 680 mb indicates cabin air leaking into the sample flow for TOPSE data (see text).

**Figure 4**. Comparison of measured and modeled OH concentrations. 5a. Direct comparison of measured and modeled OH values together with a line for 1 to 1 correlation. As can be seen the model generally tends to overestimate [OH] compared to measured values. 5b. Comparison of the ratio of measured to modeled OH values versus altitude. It can be seen that the model goes from underestimating the [OH] at low altitudes to overestimation at higher altitudes. In both plots high measured values of OH

can be seen from the first two deployments. Care should be exercised when using values from these deployments (see text).

**Figure 5**. Plot of the ratio of measured to modeled OH concentrations versus latitude. A trend of the model to overestimation of the [OH] at lower latitudes to agreement or slight underestimation at higher latitude is apparent. This type of trend has implications for unaccounted sinks of OH in the model. The "questionable" data from deployments 1 and 2 also demonstrates the trend of the model to increase the calculated [OH] with increasing latitude, however with much larger measured OH values.

**Figure 6**. Comparison of measured and modeled OH values during a low ozone event. From 1445-1530 and 1630-1710, the [$O_3$] dropped by factors of 75 and 20 respectively. At the same time the measured [OH] fell only by approximately a factor of four. As can be seen, model calculations during the same period reflect the same change in [OH] and generally agree quite well with measurements, especially for such a highly perturbed chemical environment.

**Figure 7.** Comparison of observed [$H_2SO_4$] versus altitude. Data have been separated into low (<57 °N) and high (>=57 °N) latitudes, Figures 8a and 8b, respectively. The data also have been averaged into 500 m segments. It can be seen that, overall, the largest concentrations are observed in the lower latitudes consistent with mixing of $H_2SO_4$ sources from local/regional influences. This type of mixing is also consistent with the observation that in either latitudinal region, the largest concentrations are observed at the

lowest altitudes. The seasonal dependence in the high latitudes is also apparent with concentrations generally increasing through deployment 6. In both latitude sets, deployment 7 shows a dramatic decrease in values at all altitudes. The large excursions in deployments 3 and 6 could possibly be due to volcanic activity, although little correlation with measured $SO_2$ values was noted.

**Figure 8**. Evidence of particle nucleation observed during a $H_2SO_4$ event. From 2015-2025 the [$H_2SO_4$] increased by over a factor of 10. The correlation with UCN is clearly evident, indicating the presence of more aged ultra fine particles. The peaks for the 3-4 nm UCN indicate the presence of very young, recently nucleated particles, which have not had time to grow or become incorporated into larger particles.

**Figure 9**. Typical layering of observed MSA. Plots of measured [MSA] versus time and versus altitude, figures 10a and 10b respectively, for an MSA event. The strong layering of MSA can be seen. Events such as this one were usually accompanied by other species such as $NO_x$, $NO_y$ which indicate that the MSA may have an industrial source.

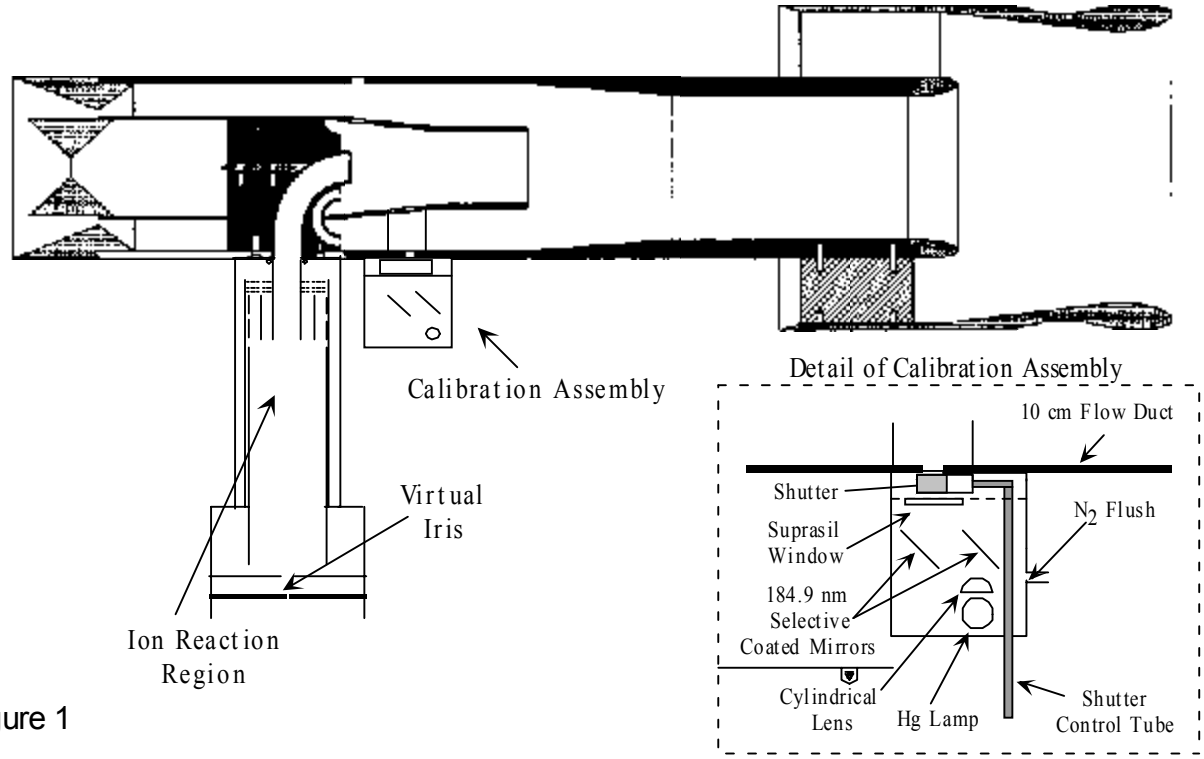
Calibration Assembly
Virtual
Iris
Ion Reaction
Region
Detail of Calibration Assembly
10 cm Flow Duct
Shutter
$N_2$ Flush
Suprasil
Window
184.9 nm
Selective
Coated Mirrors
Cylindrical
Lens
Hg Lamp
Shutter
Control Tube

Figure 1

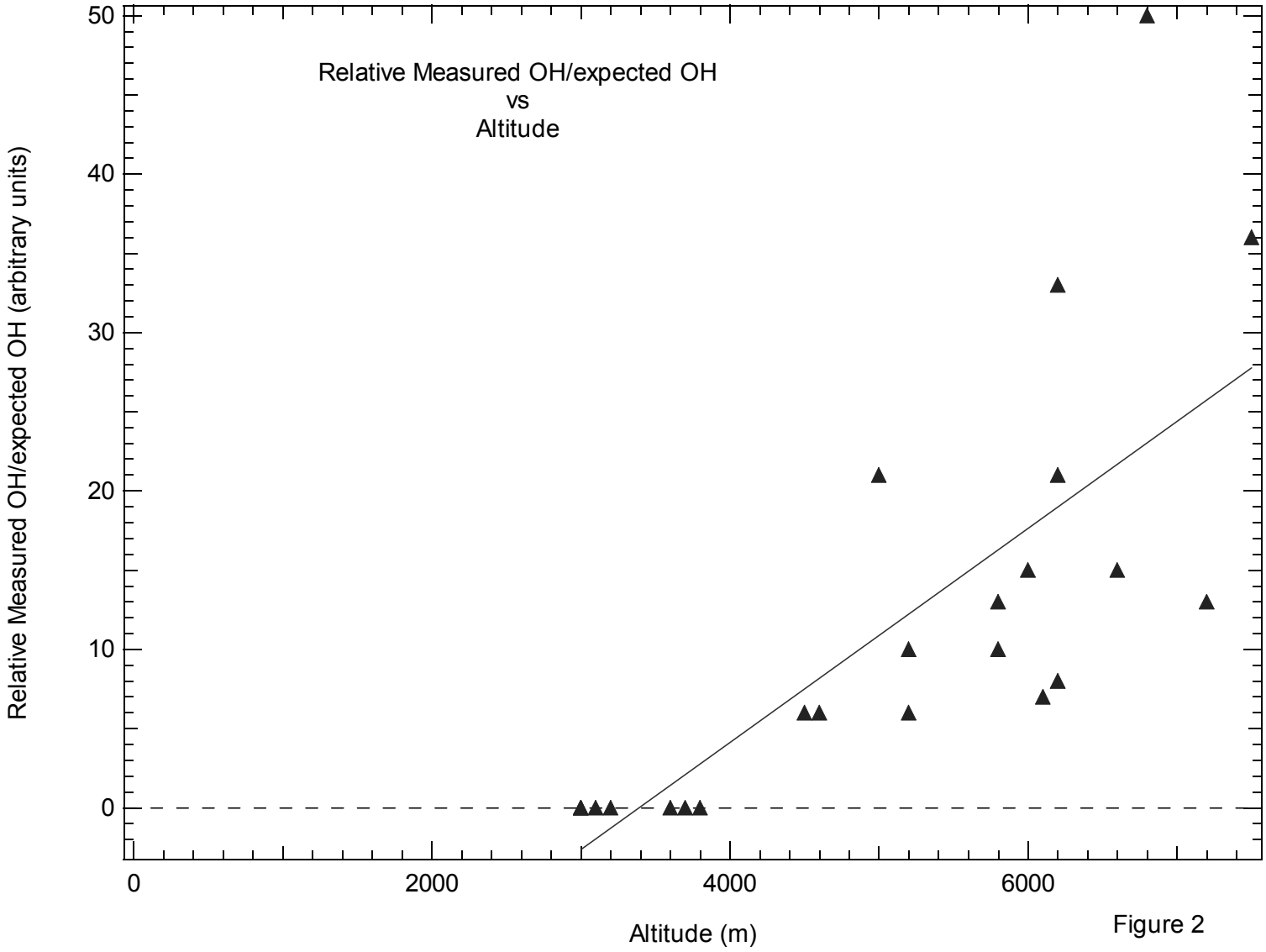
Relative Measured OH/expected OH
vs
Altitude
Relative Measured OH/expected OH (arbitrary units)
50
40
30
20
10
0
0
2000
4000
6000
Altitude (m)

Figure 2

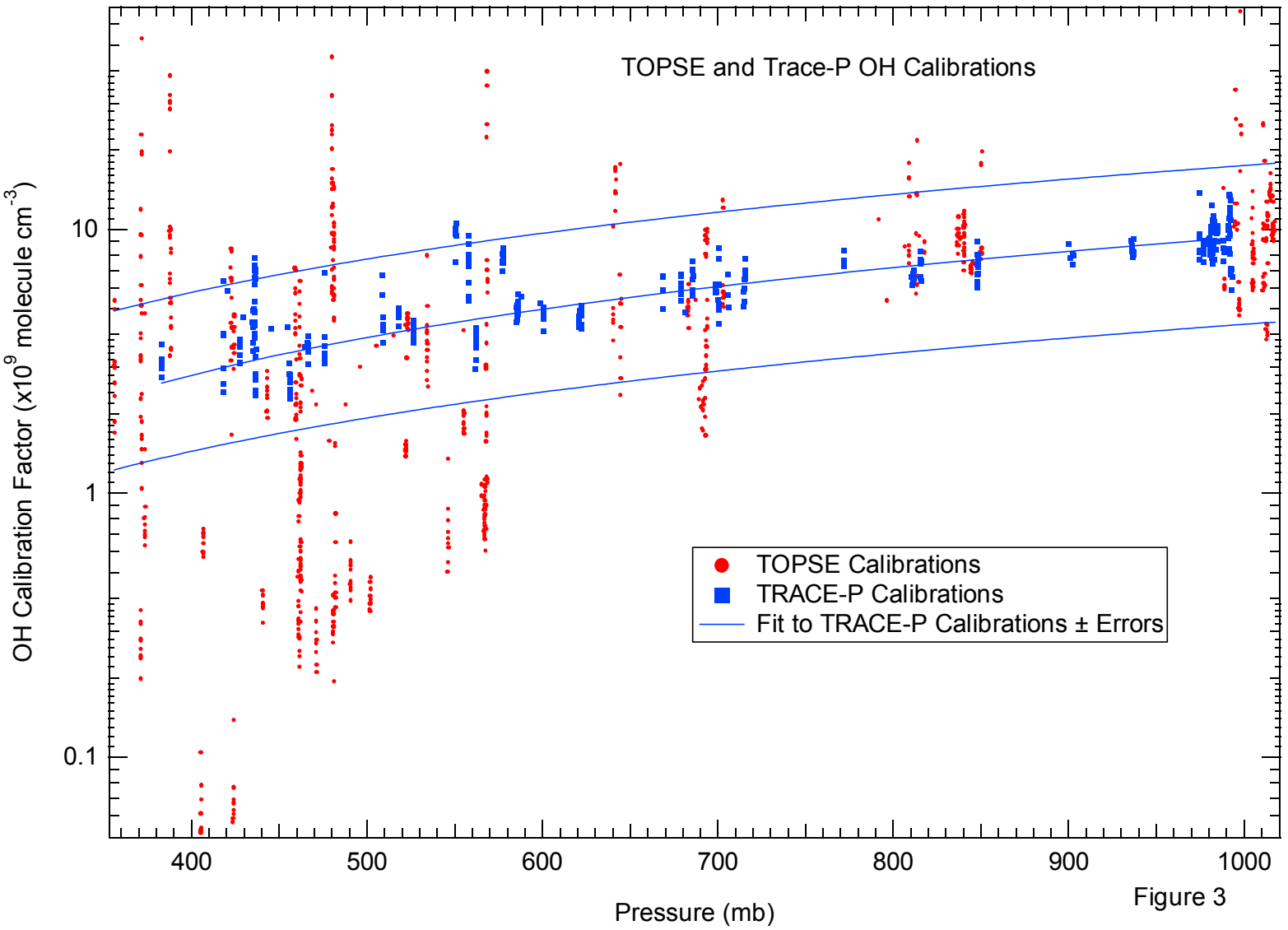
TOPSE and Trace-P OH Calibrations
OH Calibration Factor (x10^9 molecule cm^-3)
10
1
0.1
400
500
600
700
800
900
1000
Pressure (mb)
TOPSE Calibrations
TRACE-P Calibrations
Fit to TRACE-P Calibrations ± Errors

Figure 3

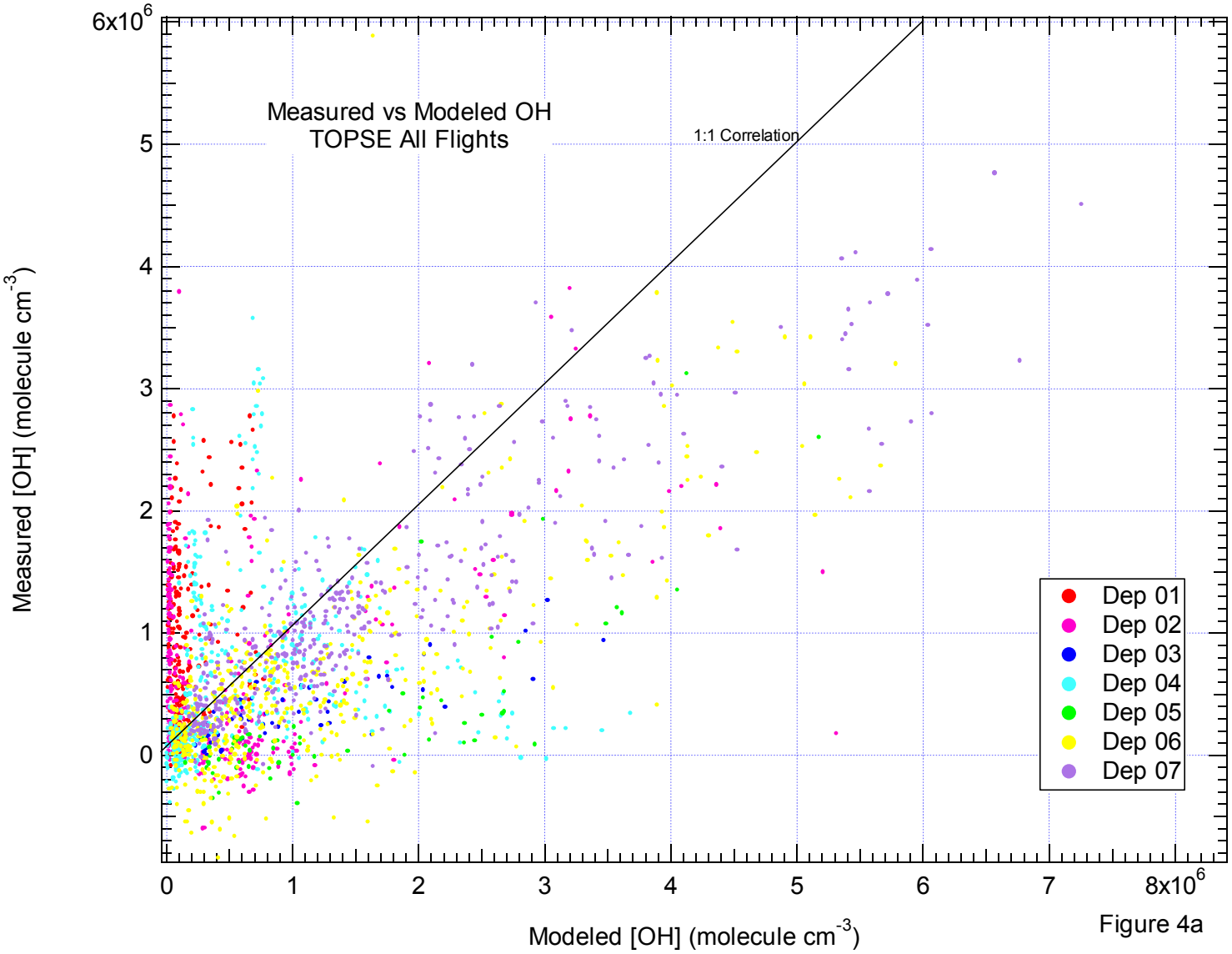
Measured vs Modeled OH
TOPSE All Flights
1:1 Correlation
Dep 01
Dep 02
Dep 03
Dep 04
Dep 05
Dep 06
Dep 07
Measured [OH] (molecule cm-3)
Modeled [OH] (molecule cm-3)
6x10^6
8x10^6
0
1
2
3
4
5
6
7

Figure 4a

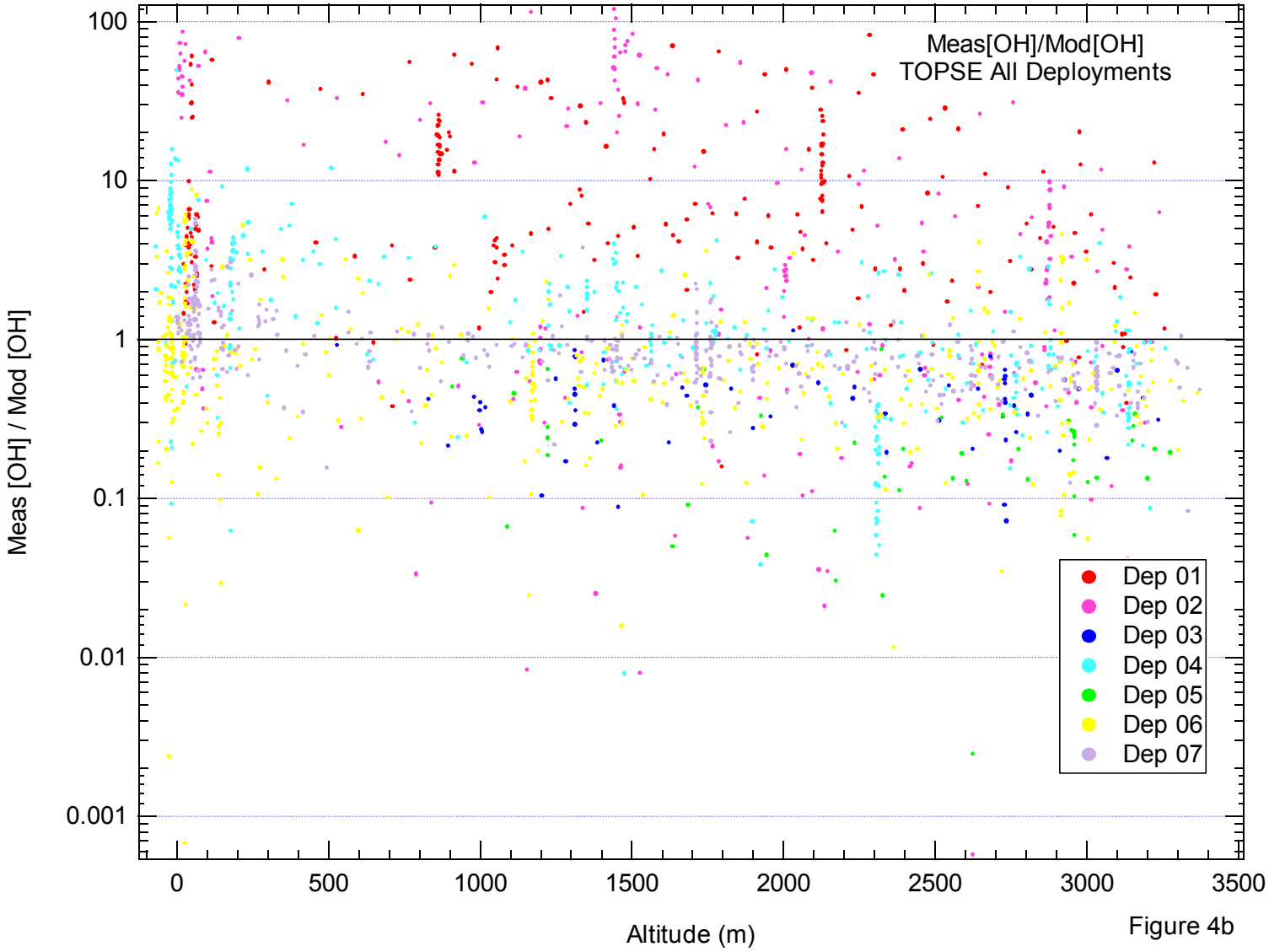
Meas[OH]/Mod[OH]
TOPSE All Deployments
Meas [OH] / Mod [OH]
Altitude (m)
100
10
1
0.1
0.01
0.001
0
500
1000
1500
2000
2500
3000
3500
Dep 01
Dep 02
Dep 03
Dep 04
Dep 05
Dep 06
Dep 07

Figure 4b

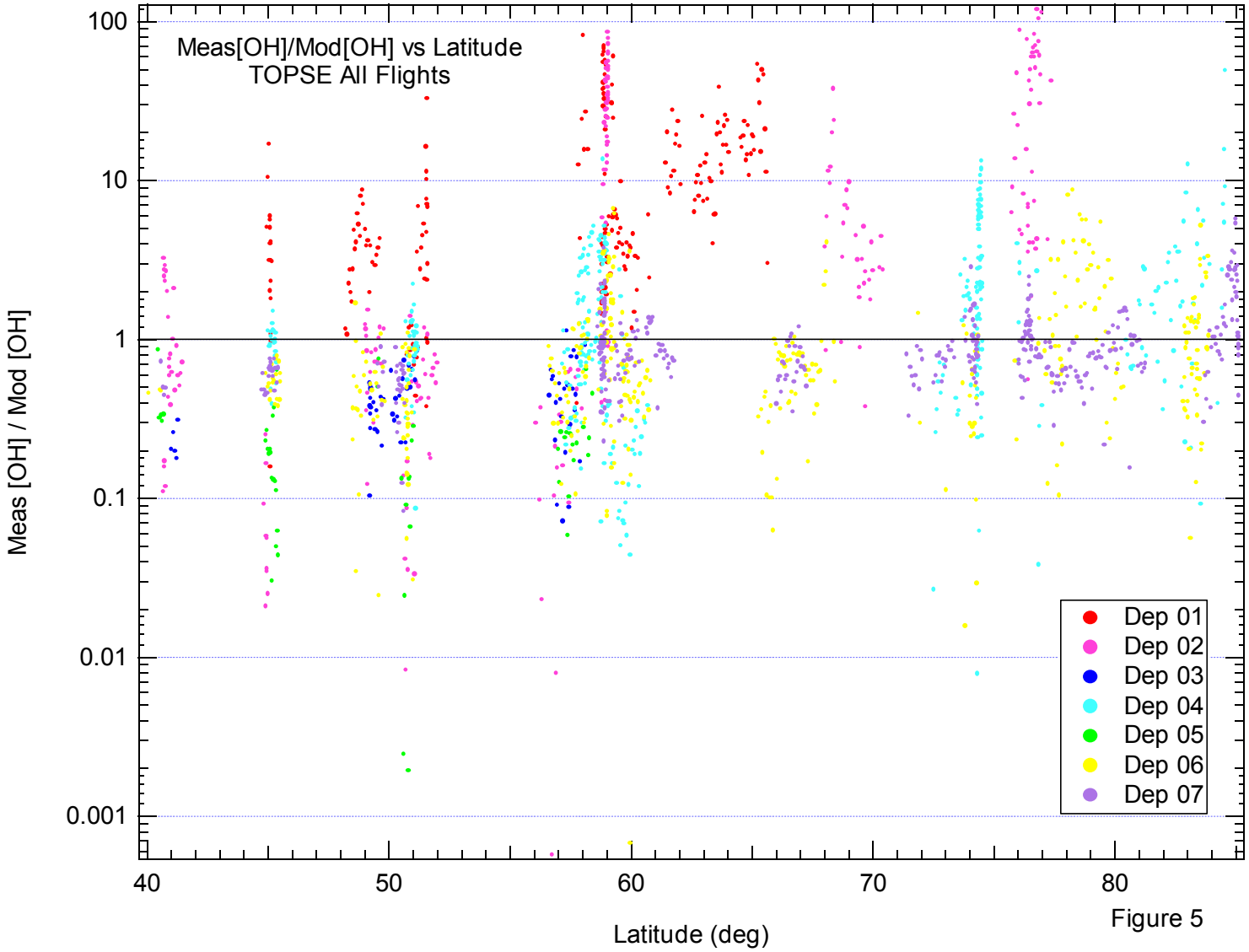
Meas[OH]/Mod[OH] vs Latitude
TOPSE All Flights
Meas [OH] / Mod [OH]
100
10
1
0.1
0.01
0.001
40
50
60
70
80
Latitude (deg)
Dep 01
Dep 02
Dep 03
Dep 04
Dep 05
Dep 06
Dep 07

Figure 5

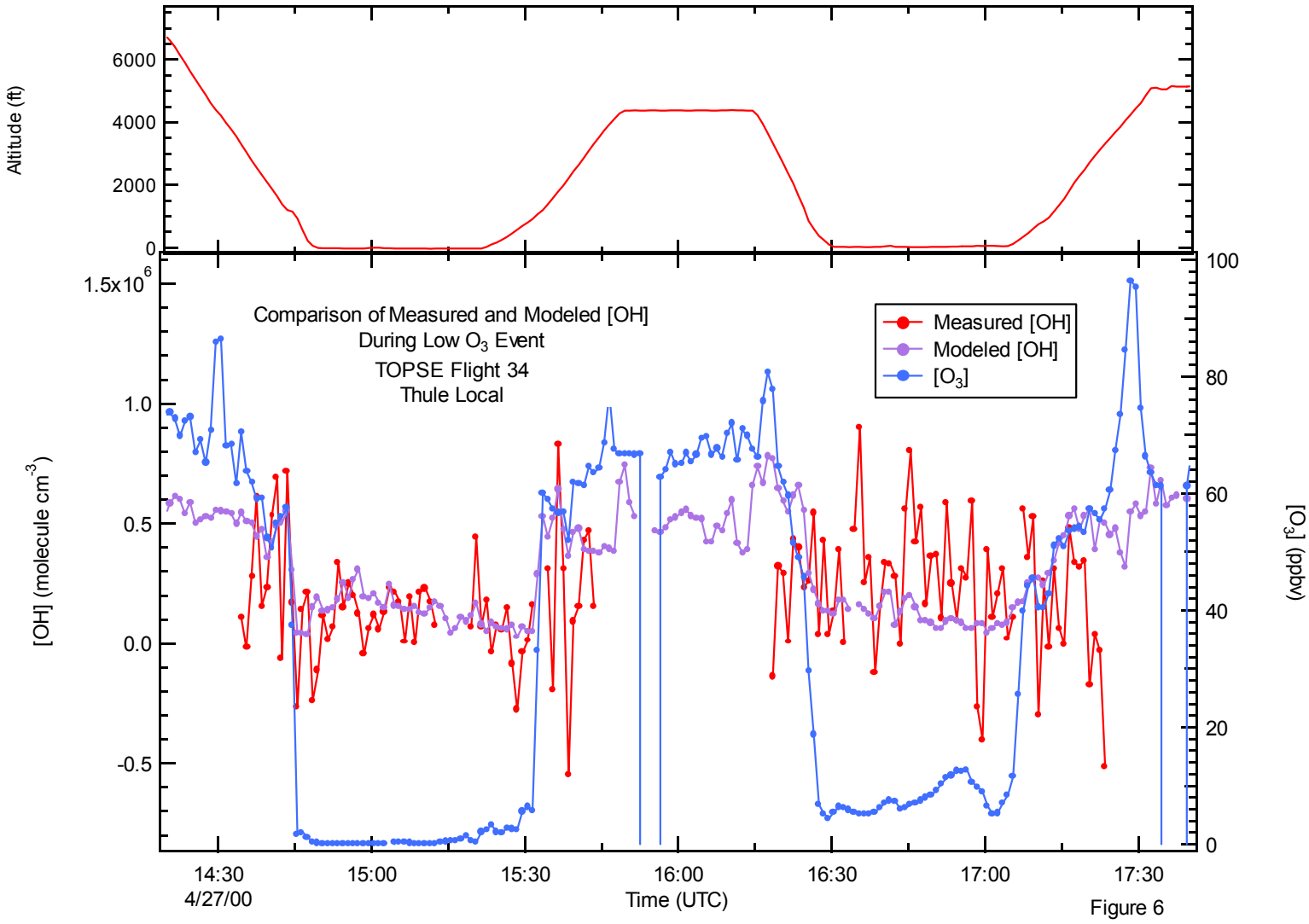
Altitude (ft)
6000
4000
2000
0
Comparison of Measured and Modeled [OH]
During Low $O_3$ Event
TOPSE Flight 34
Thule Local
Measured [OH]
Modeled [OH]
[$O_3$]
[OH] (molecule $cm^{-3}$)
$1.5x10^6$
1.0
0.5
0.0
-0.5
[$O_3$] (ppbv)
100
80
60
40
20
0
14:30
4/27/00
15:00
15:30
16:00
16:30
17:00
17:30
Time (UTC)

Figure 6

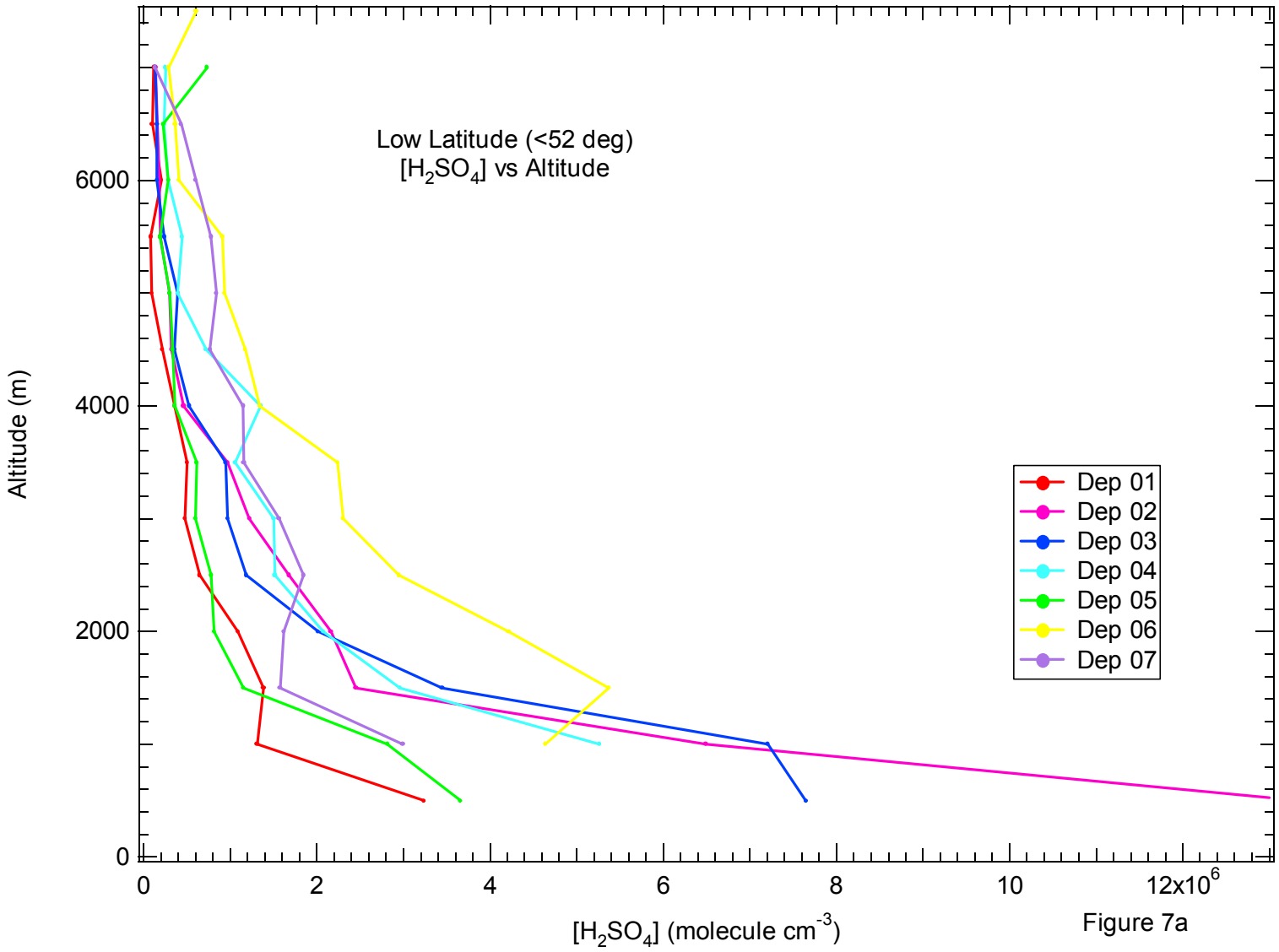
Low Latitude (<52 deg)
[H2SO4] vs Altitude
Altitude (m)
0
2000
4000
6000
0
2
4
6
8
10
12x10^6
[H2SO4] (molecule cm^-3)
Dep 01
Dep 02
Dep 03
Dep 04
Dep 05
Dep 06
Dep 07

Figure 7a

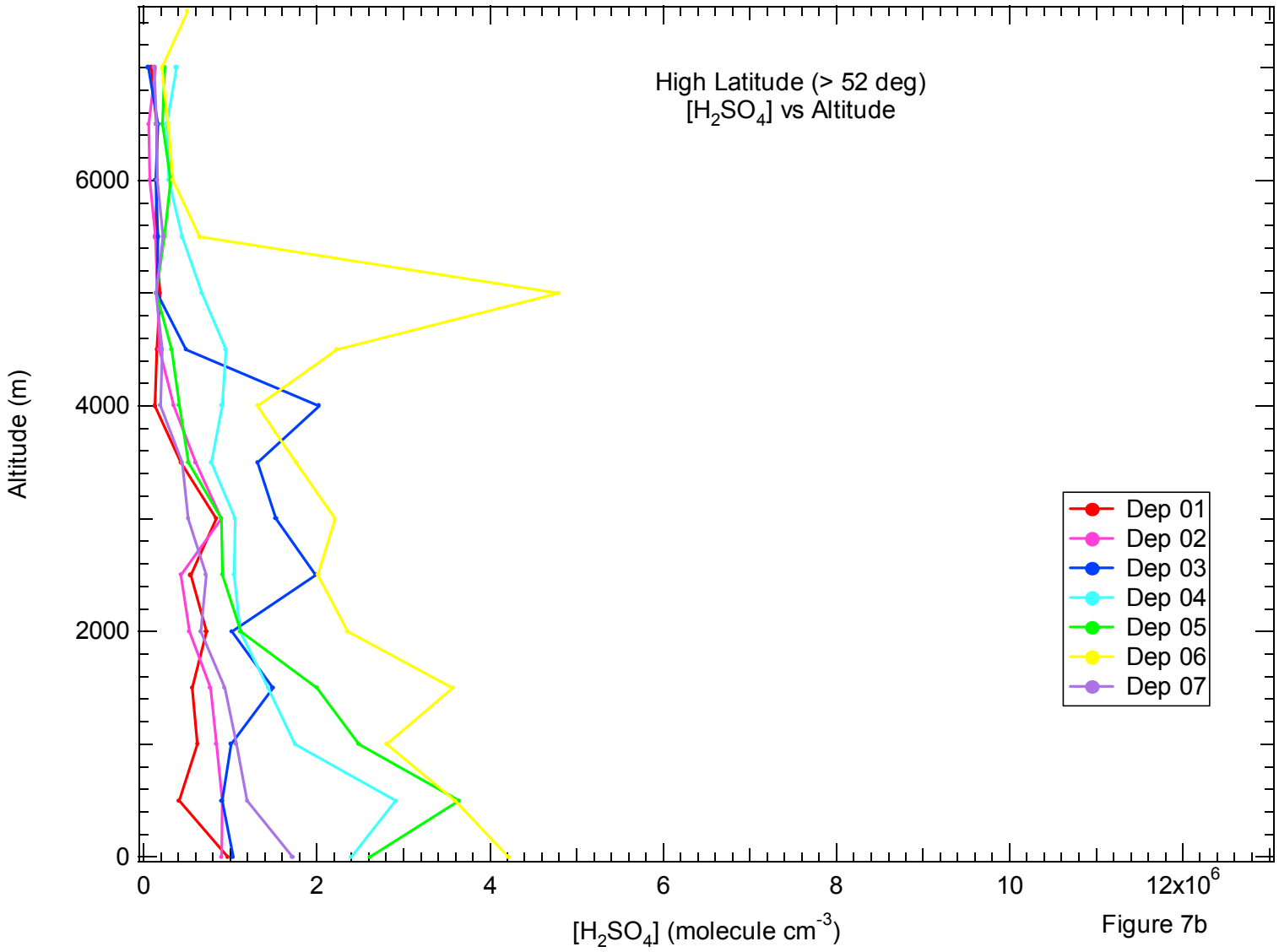
High Latitude (> 52 deg)
[H2SO4] vs Altitude
Altitude (m)
0
2000
4000
6000
0
2
4
6
8
10
12x10^6
[H2SO4] (molecule cm^-3)
Dep 01
Dep 02
Dep 03
Dep 04
Dep 05
Dep 06
Dep 07

Figure 7b

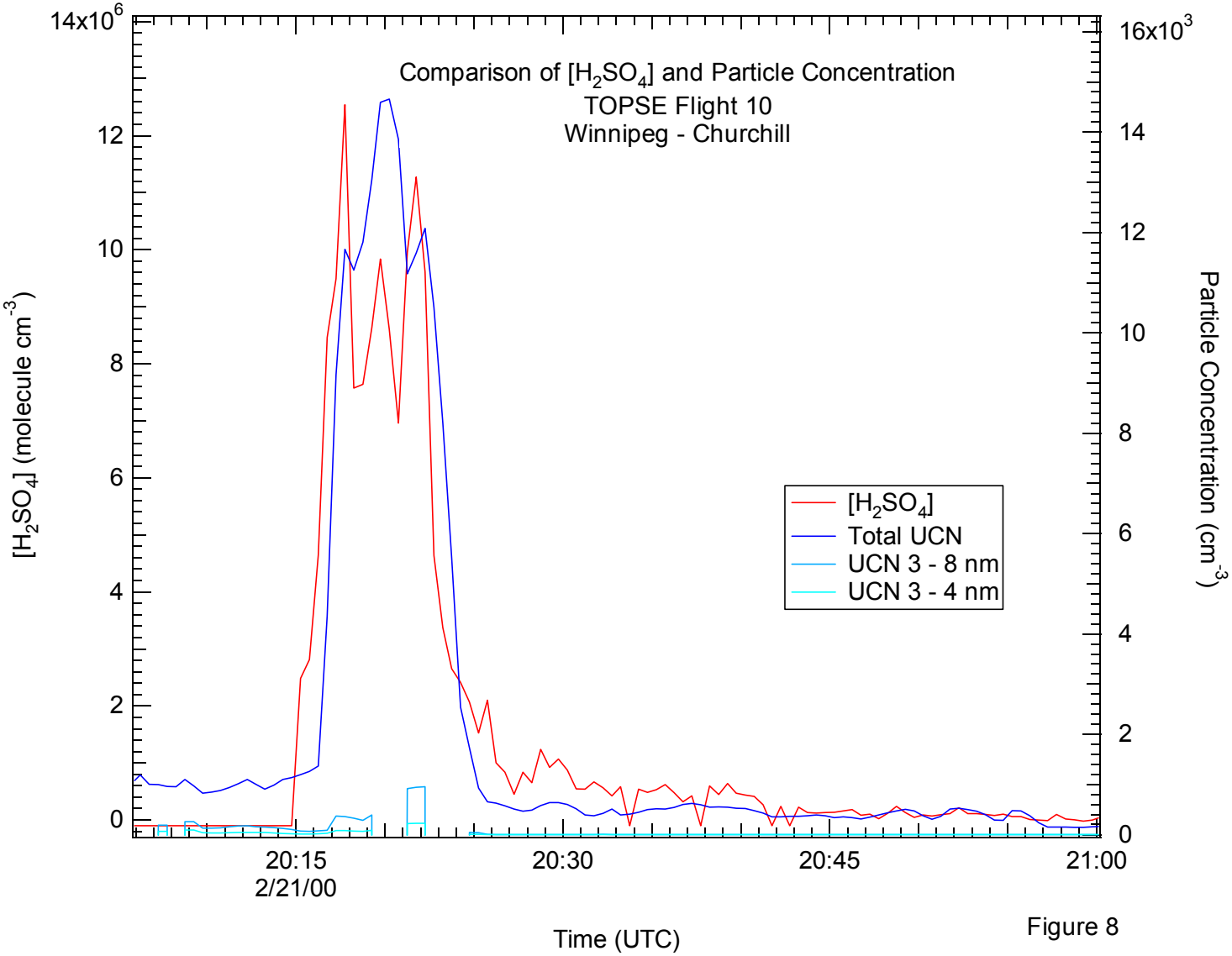
Comparison of [H2SO4] and Particle Concentration
TOPSE Flight 10
Winnipeg - Churchill
[H2SO4]
Total UCN
UCN 3 - 8 nm
UCN 3 - 4 nm
14x10^6
12
10
8
6
4
2
0
16x10^3
14
12
10
8
6
4
2
0
[H2SO4] (molecule cm^-3)
Particle Concentration (cm^-3)
20:15
2/21/00
20:30
20:45
21:00
Time (UTC)

Figure 8

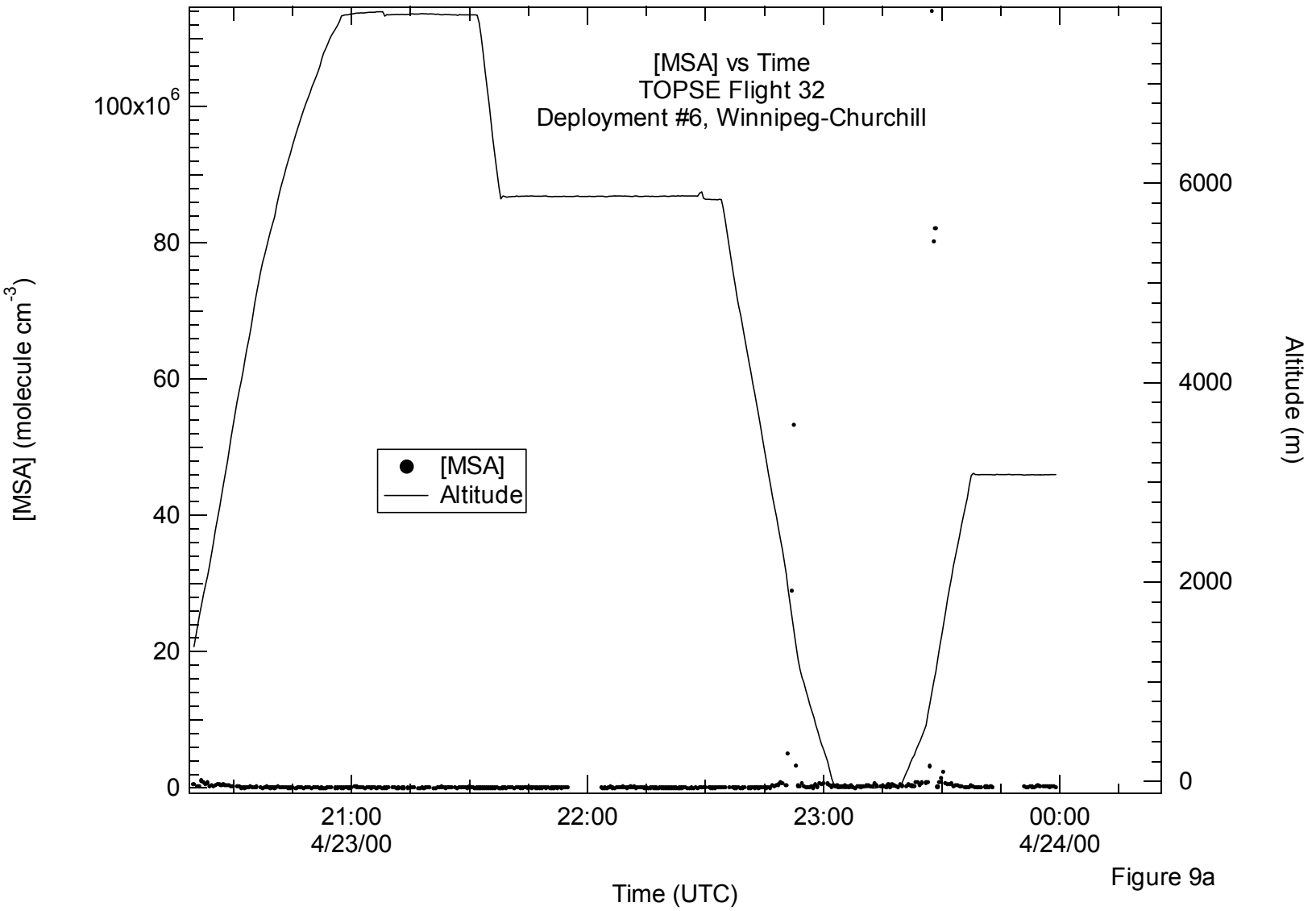
[MSA] vs Time
TOPSE Flight 32
Deployment #6, Winnipeg-Churchill
100x10^6
80
60
40
20
0
[MSA] (molecule cm^-3)
[MSA]
Altitude
6000
4000
2000
0
Altitude (m)
21:00
4/23/00
22:00
23:00
00:00
4/24/00
Time (UTC)

Figure 9a

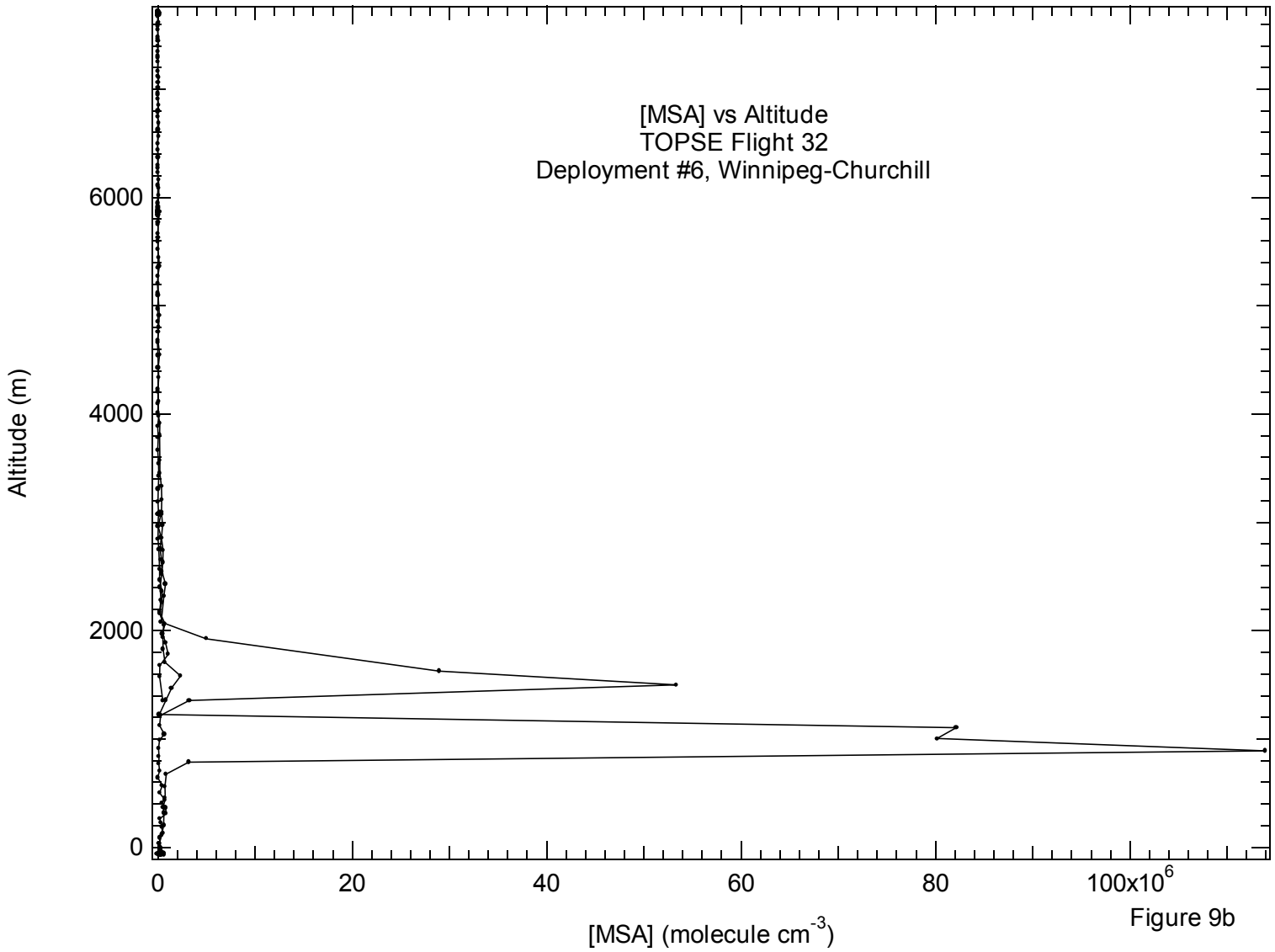
[MSA] vs Altitude
TOPSE Flight 32
Deployment #6, Winnipeg-Churchill
Altitude (m)
0
2000
4000
6000
0
20
40
60
80
100x10^6
[MSA] (molecule cm^-3)

Figure 9b